

Combining recurrent and residual learning for deforestation monitoring using multitemporal SAR images

Carla Nascimento Neves^a, Raul Queiroz Feitosa^b, Mabel X. Ortega Adarme^b, Gilson Antonio Giraldi^a

^a*National Laboratory for Scientific Computing, Petropolis, RJ, Brazil*

^b*Pontifical Catholic University of Rio de Janeiro, 22451-900 Rio de Janeiro, Brazil*

Abstract

With its vast expanse, exceeding that of Western Europe by twice, the Amazon rainforest stands as the Earth’s largest forest, holding immense importance in global climate regulation. Yet, deforestation detection from remote sensing data in this region poses a critical challenge, often hindered by the persistent cloud cover that obscures optical satellite data for much of the year. Addressing this need, this paper proposes three deep-learning models tailored for deforestation monitoring, utilizing SAR (Synthetic Aperture Radar) multitemporal data moved by its independence on atmospheric conditions. Specifically, the study proposes three novel recurrent fully convolutional network architectures—namely, RRCNN-1, RRCNN-2, and RRCNN-3—crafted to enhance the accuracy of deforestation detection. Additionally, this research explores replacing a bitemporal with multitemporal SAR sequences, motivated by the hypothesis that deforestation signs quickly fade in SAR images over time. A comprehensive assessment of the proposed approaches was conducted using a Sentinel-1 multitemporal sequence from a sample site in the Brazilian rainforest. The experimental analysis confirmed that analyzing a sequence of SAR images over an observation period can reveal deforestation spots undetectable in a pair of images. Notably, experimental results underscored the superiority of the multitemporal approach, yielding approximately a 5% enhancement in F1-Score across all tested network architectures. Particularly the RRCNN-1 achieved the highest accuracy and also boasted half the processing time of its closest counterpart.

Keywords: Remote sensing, Deforestation detection, SAR images

1. Introduction

Remote sensing refers to acquiring information about an object from a remote location. This term is frequently employed to describe the imaging of the Earth’s surface from an elevated perspective, such as via satellite (Parelius, 2023). Multitemporal remote sensing data can offer wide information for land change monitoring (Shi et al., 2020; Ban & Yousif, 2016).

Change detection captures spatial differences in the state of an object by observing it at different times (Singh, 1989). In the Remote Sensing context, its purpose is to monitor environmental changes by jointly processing a set of images of the same geographical area acquired at different dates, which is essential for the management of natural resources, the conservation of ecosystems and biodiversity as well as decision support for sustainable development (Asokan & Anitha, 2019).

Change detection using remote sensing imagery assumes a crucial function in numerous fields of applications, including disaster monitoring (Zheng et al., 2021b), biodiversity study (Newbold et al., 2015), desertification (Dawelbait & Morari, 2012), urbanization process (Han et al., 2017) and deforestation detection (De Bem et al., 2020), which is the focus of this research.

Email addresses: cneves@lncc.br (Carla Nascimento Neves), raul@ele.puc-rio.br (Raul Queiroz Feitosa), mortega@ele.puc-rio.br (Mabel X. Ortega Adarme), gilson@lncc.br (Gilson Antonio Giraldi)

Among these applications, preserving the rainforests is critical in maintaining the health and stability of our planet’s ecosystems. In particular, the Amazon rainforest, the Earth’s largest forest, has suffered increasing deforestation rates in recent years, with Brazil being the country where the most significant statistics are concentrated (Giljum et al., 2022; Amin et al., 2019).

The Brazilian government tracks deforestation in the Amazon region through systematic satellite monitoring. For example, the Amazon Deforestation Monitoring Project (PRODES¹) provides annual reports about deforestation in the Brazilian Legal Amazon (BLA) since 1988 (Valeriano et al., 2004). One notable limitation of PRODES and several other deforestation monitoring systems is their dependency on optical data. Optical data are frequently hindered by cloud cover throughout most of the year in tropical regions (Doblas et al., 2020)

Various techniques have been addressed to create change maps for deforestation detection, including simple differencing (Stauffer & McKinney, 1978), change vector analysis (Perbet et al., 2019) and traditional machine learning techniques like Support Vector Machine (Reis et al., 2020), Principal Component Analysis (Sule & Wood, 2020), Random Forest (Hethcoat et al., 2020), Maximum Likelihood (Diniz et al., 2022) and distance-based classifiers (Nicolau et al., 2021).

Apart from these methods and their variations, numerous publications have incorporated deep learning in remote sensing change detection and demonstrated their superiority over conventional change detection methods Bai et al. (2022).

Among the recent researches with deep learning solutions for change detection, Autoencoders, U-Net and its variants (Li et al., 2022; Zheng et al., 2021a), Recurrent Networks (Fang et al., 2023; Shi et al., 2022), Generative Adversarial Networks (Zhao et al., 2020), and Transformer-based networks (Chen et al., 2021; Wang et al., 2022) are included.

A current research line Panuju et al. (2020) focuses on combining different techniques to improve change detection accuracy in remote sensing. Moreover, Parelius (2023) points out that the growing abundance of satellite imagery offers an opportunity to shift focus from the traditional bitemporal change detection methods used in previous studies to models that exploit longer time-series images. This approach allows for the incorporation of a richer set of data for change detection, a perspective that has been relatively underexplored until now, as emphasized in Parelius (2023).

The present study follows this trend and seeks to develop solutions for change detection with remote sensing data, specifically for deforestation monitoring, by employing multitemporal SAR data and combinations of different deep learning techniques. This paper proposes three recurrent fully convolutional deep networks for pixel-wise deforestation detection from SAR images. Furthermore, this study assesses the application of image sequences instead of bitemporal SAR image pairs for deforestation detection. This approach is inspired by the hypothesis that deforestation signs in tropical forests tend to rapidly diminish in SAR imagery due to the natural process of forest regeneration. Consequently, deforestation detection becomes increasingly challenging when bi-temporal image acquisition intervals are too widely apart. By harnessing a sequence of multiple images captured between such intervals, we substantially enhance the prospects of accurate and timely deforestation detection.

The main contributions of this work are:

- Development of novel deep learning based solutions for automatic deforestation mapping and comparison with state-of-art methods.
- Addressing underexplored aspects in change detection literature, including the use of longer multitemporal data sequences.
- Experimental analysis of the proposed methods using SAR data provided by Sentinel-1 from a sample site of the Amazon forest.

This paper is organized as follows. Section 2 discusses the recent research and also the gaps in change detection with deep learning. Section 3 provides the theoretical background on the deep learning techniques

¹<http://www.obt.inpe.br/OBT/assuntos/programas/amazonia/prodes>

that inspired the architectures developed in the present work and Section 4 introduces the proposed models. Section 5 presents the employed data, the experimental setup, and the architectures used for comparison. Section 6 shows and discusses the experimental results. Finally, Section 7 presents the main conclusions drawn from this study.

2. Related Works

With the continuous advancement of Deep Learning methods within computer vision, their application has been extended to the problem of change detection in Remote Sensing due to their ability to capture complex and hierarchical features present in the data (Parelius, 2023). Hence, this section will discuss recent works with deep learning solutions for change detection problems.

The U-Net encoder-decoder architecture and its variants are commonly employed for change detection tasks among the reviewed models. For instance, Zheng et al. (2021a) introduced the Cross-Layer Convolutional Neural Network (CLNet), which is a modified U-Net with Cross-Layer Blocks (CLB) incorporated to integrate multi-scale features and multi-level contextual information by temporarily splitting the input into two parallel asymmetrical branches using different convolution strides and concatenating the feature maps from the two branches. Experiments were conducted on two building change detection datasets: the Learning Vision and Remote Sensing Laboratory building change detection (LEVIR-CD) and WHU-CD, reaching superior performance compared to several state-of-the-art methods.

Wang et al. (2022) proposed the U-Net-like Visual Transformer for Change Detection (UVACD) for bitemporal image change detection. This network uses a CNN backbone for extracting semantic information followed by a visual transformer for feature enhancement that constructs change intensity tokens to complete the temporal information interaction and suppress irrelevant information weights to help obtain more distinguishable change features. The experiments were conducted on the WHU-CD and LEVIR-CD datasets. The authors reported a Precision of 94.58%, a Recall of 91.17%, an F1 score of 92.84%, and an IoU of 86.64% on the WHU-CD. UVACD outperformed some previous state of the art change detection methods in the experimental results.

U-Nets variants proposed in the literature take the form of a double-stream architecture. One example is the Densely Attentive Refinement Network (DARNet) introduced in Li et al. (2022) to improve change detection on bitemporal very-high-resolution (VHR) remote sensing images. DARNet has a dense skip connections module between the encoder-decoder architecture, which combines features from various levels. A hybrid attention module is inserted at the skip connections level to combine temporal, spatial, and channel attention. Also, a recurrent refinement module is used to refine the predicted change in the decoding process. The experimental results on the season-varying change detection (SVCD) dataset, the Sun Yat-sen University change detection (SYSU-CD) dataset, and the LEVIR-CD dataset outperformed state-of-the-art models.

Some deep learning-based models proposed for change detection include Recurrent Neural Networks (RNN) due to their ability to handle related data sequences. The sequence usually consists of images from two different time points (Parelius, 2023).

Fang et al. (2023) proposed a fine-grained Multi-Functional Radar (MFR) model followed by a multi-head attention-based bi-directional Long Short Term Memory (LSTM) network to capture relationships between successive pulses. This process uses the temporal features to predict the probability of each pulse being a change point. The simulation results achieved better performance than the compared convolutional and recurrent networks.

Shi et al. (2022) proposed a Multi-path Convolutional LSTM (MP-ConvLSTM) by combining LSTM and a CNN for change detection with bi-temporal hyperspectral images. A Siamese CNN was adopted to reduce the dimensionality of the images and extract preliminary features. A Convolutional LSTM was used to learn multi-level temporal dependencies among them. The MP-ConvLSTM was evaluated using four publicly available hyperspectral datasets acquired by the Earth Observing-1 (EO-1) Hyperion and obtained superior results than several state-of-the-art change detection algorithms, also exhibiting better trade-off between complexity and accuracy in general.

Papadomanolaki et al. (2019) presented a framework for urban change detection that combines a fully convolutional network (FCN) similar to U-Net for feature representation and a recurrent network for tem-

poral modeling. The U-Net-based encoder–decoder architecture has a convolutional LSTM block added at all levels of the encoder. The authors evaluated the performance of this network using an ensemble cross-validation strategy on bi-temporal data from Onera Satellite Change Detection (OSCD) Sentinel-2 dataset (SAR data). The U-Net+LSTM model outperformed the regular U-Net.

Strategies using residual learning (He et al., 2016) to facilitate gradient convergence are also applied with FCN approaches for change detection since such a combination helps obtain a more comprehensive range of information (Khelifi & Mignotte, 2020; Shafique et al., 2022).

Basavaraju et al. (2022) introduced UCDNet, the Urban Change Detection Network. This model is based on an encoder-decoder architecture, using a version of spatial pyramid pooling (SPP) blocks for extracting multiscale features and residual connections for introducing additional maps of feature differences between the streams at each level of the encoder to improve change localization, aiming to acquire better predictions while preserving the shape of changed areas. UCDNet uses a proposed loss function, a combination of weighted class categorical cross-entropy (WCCE) and modified Kappa loss. The authors evaluated the network on bi-temporal multispectral Sentinel-2 satellite images from Onera Satellite Change Detection (OSCD), obtaining better results than the models used for comparison.

The Multiscale Residual Siamese Network fusing Integrated Residual Attention (IRA-MRSNet), proposed by Ling et al. (2022), introduced multi-resolution blocks that combine convolutions with kernels of different sizes to extract deep semantic information and features at multiple scales. In addition, this network utilizes an attention unit connecting the encoder and the decoder. In experiments conducted on Seasonal Change Detection Dataset (CDD) the network outperformed the counterpart methods.

Peng et al. (2019) presented an improved U-Net++ design where change maps could be learned from scratch using available annotated datasets. The authors adopted the U-Net++ model with dense skip connections as the backbone for learning multiscale feature maps from several semantic layers. Residual blocks are employed in the convolution unit, aiming for better convergence. Deep supervision is implemented by using multiple side-output fusion (MSOF) to combine change maps from different semantic levels, generating a final change map. They used the weighted binary cross-entropy loss and the dice coefficient loss to mitigate the impact of class imbalance. The performance of the proposed CD method was verified on a VHR satellite image dataset and achieved a superior performance than the related methods.

Recent studies proposed change detection techniques by combining residual and recurrent learnings. For instance, Khankeshizadeh et al. (2022) presented FCD-R2U-Net, a forest change detection that includes a module for producing an enhanced forest fused difference image (EFFDI), to achieve a more efficient distinction of changes, followed by (Recurrent Residual U-Net) R2U-Net, applied to segment the EFFDI into the changed and unchanged areas. Experimental results were conducted on four bi-temporal images acquired by the Sentinel 2 and Landsat 8 satellite sensors. The qualitative and quantitative results demonstrated the effectiveness of the proposed EFFDI in reflecting the true forest changes from the background. Regarding the qualitative results, forest changes and their geometrical details were better preserved by FCD-R2U-Net, compared with U-Net, ResU-Net, and U-Net++. The proposed network also obtained superior results in the quantitative analysis.

Moustafa et al. (2021) proposed a change detection architecture named Attention Residual Recurrent U-Net (Att R2U-Net), inspired by R2U-Net and attention U-Net. This study supports the notion that deep neural networks can learn complex features and improve change detection performance when combined with hyperspectral data. Three hyperspectral change detection datasets with class imbalance and small regions of interest were employed to evaluate the performance of the proposed method for binary and multiclass change cases. The results were compared with U-Net, ResU-Net, R2U-Net, and Attention U-Net. Att R2U-Net outperformed the counterpart methods in almost all metrics and cases.

As observed in the previously mentioned related works, in addition to developing new algorithms, combinations of available techniques are being considered to improve the accuracy of change detection in remote sensing. This is a research focus pointed out by Panuju et al. (2020).

3. Deep Learning Approaches Background

This section presents the deep learning approaches explored for constructing the change detection frameworks proposed in this study. The architectures are rooted in recurrent residual learning.

3.1. Residual Networks

To enhance the training process of deep convolutional neural networks (CNNs), Residual Networks (ResNets) were conceived based on the observation that as neural networks grow deeper, they typically encounter elevated training errors, particularly when the network’s depth becomes substantially large.

He et al. (2016) introduced the so called residual blocks (see1 equipped with skip connections or shortcuts. In a residual block, the input to a layer is combined with the output of that layer, allowing the network to pass through information without significant alteration directly. As gradients backpropagate during training, they flow nearly unaltered through these skip connections, improving the convergence at the earlier layers.

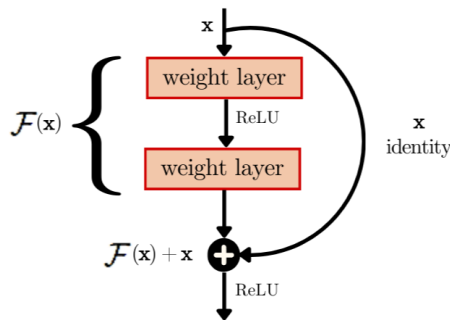


Figure 1: Residual block (RB).

Source: Adapted from He et al. (2016).

He et al. (2016) defines de building block as

$$\mathbf{y} = \mathcal{F}(\mathbf{x}, \{\mathcal{W}_i\}) + \mathbf{x} , \tag{1}$$

where \mathbf{x} and \mathbf{y} are the input and output of the layers considered and the function $\mathcal{F}(\mathbf{x}, \{\mathcal{W}_i\})$ denotes the residual mapping with learnable weights assembled in \mathcal{W}_i . The example in Figure 1 has two layers, so $\mathcal{F} = W_2 \sigma(W_1 \mathbf{x})$, with σ representing the rectified linear unit (ReLU) activation function (Nair & Hinton, 2010). Biases are omitted for simplifying notations. It also seen in Figure 1 that the operation $\mathcal{F} + \mathbf{x}$ is carried out by a shortcut connection and element-wise addition. These shortcut connections introduce no additional parameters and negligible computational complexity.

Inspired by the U-Net architecture and deep residual learning, Zhang et al. (2018) proposed the Deep Residual U-Net (ResU-Net). ResU-Net has three parts: The encoder consists of Residual Blocks (RB) and down-sampling operations that compress the input into compact representations. The bottleneck connects the encoder with the last part, the decoder, which comprises bilinear upsampling operations and recovers the representations to a pixel-wise categorization. In addition, skip connections link the first and last part so that information from the encoding layers is preserved and transmitted to the decoding layers.

According to Zhang et al. (2018), the deep residual units make the deep network easy to train, and the skip connections within a residual unit and between the corresponding levels of the network will facilitate information propagation without degradation, making it possible to design a deep neural network with fewer parameters.

As the present work approaches change detection, the decoder output feeds a softmax operator that delivers the posterior class probabilities for change or no change at each pixel location. The following figures show U-Net (Figure 2a) and ResU-Net (Figure 2c) variants used for deforestation detection in (Ortega et al.,

2021). The residual blocks (Figure 2b) facilitate the flow of information through the network layers, allowing the capture of relevant features of the satellite image (He et al., 2016), which is crucial for change detection.

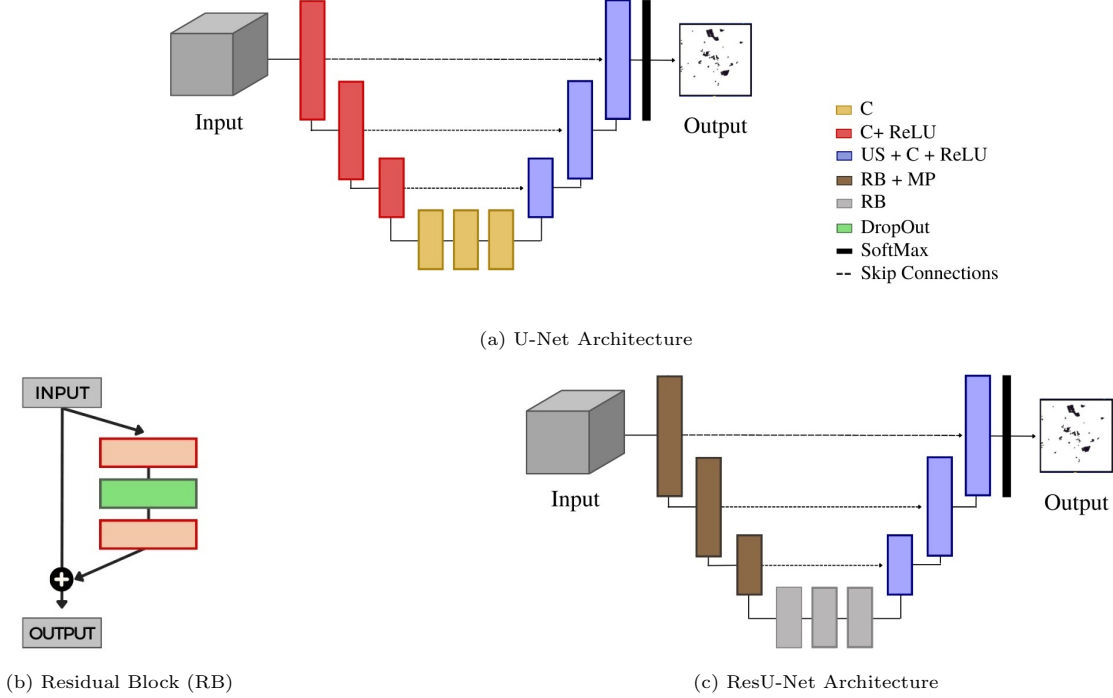


Figure 2: U-Net and ResU-Net Architectures being used for a change detection scheme. Legend: C (Convolution), MP (Max-pooling), RB (Residual Block), US (Up-sampling).

3.2. Recurrent Networks

Recurrent Neural Networks (RNNs) are designed to process sequential data, updating their internal state at each time step t while storing relevant information from prior steps (Rumelhart et al., 1986). This enables RNNs to share weights across time steps, capturing temporal patterns Goodfellow et al. (2016); Graves (2013). However, the ability to retain information over long sequences is limited in traditional RNNs due to vanishing or exploding gradients during back-propagation (Calin, 2020). The Long Short-term Memory (LSTM) (Hochreiter & Schmidhuber, 1997) networks were developed to address such limitations of conventional RNNs. They incorporate gating mechanisms that selectively allow information to flow nearly unaltered through them, allowing the capture of long-range dependencies in sequential data.

The present work employs the Convolutional LSTM Network (ConvLSTM). A ConvLSTM unit (See Figure 3) consists of inputs X_t , a cell state C_t , a hidden state H_t along with an input gate i_t , an output gate o_t and a forget gate f_t to control information flow. Due to the introduction of the convolutional structure, all the states, inputs, and intermediary outputs are three-dimensional tensors where the first two dimensions are spatial (rows and columns), and the last dimension learns feature representations (Shi et al., 2022). The input X_t and past states C_{t-1} , H_{t-1} are employed to determine the future states C_t and H_t .

The central equations are described in the sequence, with '*' denoting the convolutional operator, 'o' the Hadamard product, W the coefficient matrix, σ the sigmoid function and b the bias vector.

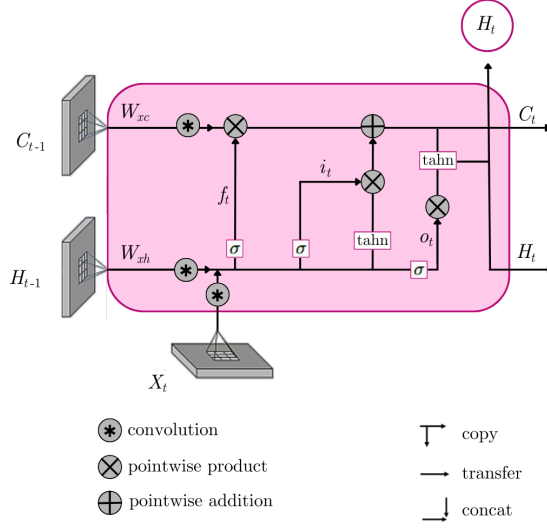


Figure 3: Inner structure of ConvLSTM

Source: Adapted from Shi et al. (2022)

$$i_t = \sigma(W_{xi} * X_t + W_{hi} * H_{t-1} + W_{ci} \circ C_{t-1} + b_i) \quad (2)$$

$$f_t = \sigma(W_{xf} * X_t + W_{hf} * H_{t-1} + W_{cf} \circ C_{t-1} + b_f) \quad (3)$$

$$C_t = f_t \circ C_{t-1} + i_t \circ \tanh(W_{xc} * X_t + W_{hc} * H_{t-1} + b_c) \quad (4)$$

$$o_t = \sigma(W_{xo} * X_t + W_{ho} * H_{t-1} + W_{co} \circ C_t + b_o) \quad (5)$$

$$H_t = o_t \circ \tanh(C_t) \quad (6)$$

According to Shi et al. (2022), the focus when using ConvLSTM for a change detection task is on capturing short-term temporal dependencies that accentuate bands capable of detecting changes while attenuating bands with less informative content. ConvLSTM recognizes and analyzes the multitemporal changes in image sequences by capturing temporal dependencies and incorporating temporal features into the change detection process. Consequently, the hidden states H_t of the ConvLSTM output can be extracted as representative features of changes.

Considering this ability, convLSTM has been used in applications involving sequential images, such as detection of changes in hyperspectral images (Shi et al., 2022), detection of urban changes (Papadomanolaki et al., 2019) and deforestation detection (Masolele et al., 2021).

3.3. Recurrent Residual Networks

According to Yue et al. (2018), residual learning and shortcut connections can effectively mitigate the exploding and vanishing gradient issues in long-term backpropagation. Bringing together the residual learning described in Section 3.1 and the recurrent learning presented in Section 3.2, Recurrent Residual Neural Networks have been proposed in the literature. Some examples include the Hybrid Residual LSTM (HRL) used for sequence classification (Wang & Tian, 2016), R2U++ (Mubashar et al., 2022) and the Deep Recurrent U-Net (DRU-Net) (Kou et al., 2019) proposed for medical image segmentation.

A particular recurrent residual network called R2U-Net (Alom et al., 2019) takes the U-Net architecture and the residual blocks of ResU-Net (Figure 2) as a starting point and includes the recurrent learning. This model combines recurrent convolutional operations with the residual blocks in Recurrent Residual Convolutional Units (RRCU - Figure 4a) to replace the regular convolutional layers in the U-Net. Each

RRCU has two Recurrent Convolutional Layers (RCL), and the input of the residual block is added to the output of the second RCL unit.

The unfolded RCL (Figure 4b) for t time steps is a feed-forward sub-network of depth $t + 1$. The figure exemplifies an RCL with $t = 2$, referring to the recurrent convolutional operation that includes one single convolution layer followed by two sub-sequential recurrent convolutional layers.

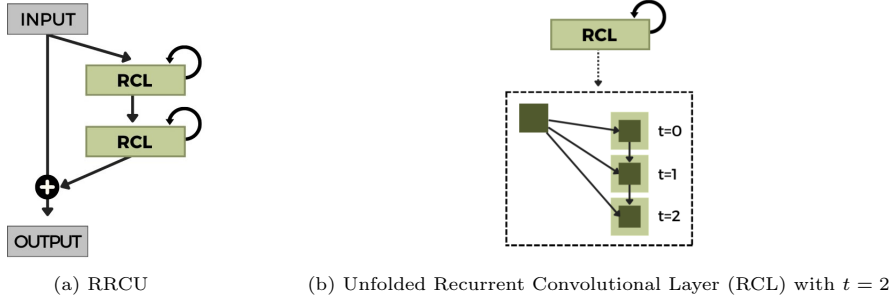


Figure 4: Recurrent Residual Convolutional Unit (RRCU)

The following mathematical explanation of an RCL unit is adapted from Liang & Hu (2015). For a unit located at (i, j) on the k -th feature map in an RCL, the net input, $z_{ijk}(t)$ at a step t , is formulated as:

$$z_{ijk}(t) = (\mathbf{w}_k^f)^T \mathbf{x}^{f(i,j)}(t) + (\mathbf{w}_k^r)^T \mathbf{x}^{r(i,j)}(t-1) + b_k, \quad (7)$$

where $\mathbf{x}^{f(i,j)}(t)$ and $\mathbf{x}^{r(i,j)}(t-1)$ represents the feedforward and recurrent input, respectively. They correspond to the vectorized patches centered at (i, j) of the feature maps in the current and previous layer. The terms \mathbf{w}_k^f and \mathbf{w}_k^r represent the vectorized feed-forward weights and recurrent weights, respectively, and b_k is the bias. The first term in Eq. 7 is used in standard CNN and the recurrent connections induce the second term. The activity or state of this unit is a function of $z_{ijk}(t)$, where σ is the ReLU:

$$\sigma(z_{ijk}(t)) = \max(z_{ijk}(t), 0) \quad (8)$$

The RRCU proposed by Alom et al. (2019) uses the RCL in a Residual Block, as shown in Figure 4a. Considering x_l as the input in the l^{th} layer of an RRCU, the output of this unit, x_{l+1} , can be calculated as:

$$x_{l+1} = x_l + F(x_l, w_l), \quad (9)$$

where $F(x_l, w_l)$ is the output of the last RCL, expressed as

$$F(x_l, w_l) = \sigma(z_{ijk}^l(t)) = \max(z_{ijk}^l(t), 0). \quad (10)$$

Figure 5 shows a R2U-Net architecture with three encoding and decoding levels and a bottleneck between these stages, employing RRCUs.

Recurrent residual architectures derived from R2U-Net, including FCD-R2U-Net (Khankeshizadeh et al., 2022) and Att R2U-Net (Moustafa et al., 2021) have been used for change detection tasks. Alom et al. (2019) and Kou et al. (2019) state that the inclusion of RCLs in residual units further enhances the ability to handle deeper architectures. Also, the process of collecting and combining information from different time-steps in a recurrent neural network allows the model to capture dependencies and patterns over longer sequences of data. This feature accumulation process leads to more comprehensive feature representations and helps the model extract very low-level features from the data, which are crucial for segmentation tasks across various modalities.

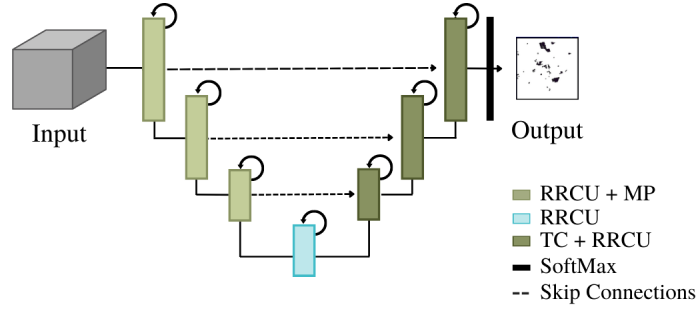


Figure 5: R2U-Net Architecture for change detection. Legend: MP (Max-pooling), TC (Transpose Convolution), RRCU (Recurrent Residual Convolutional Unit)

4. Proposed Architectures

This section presents the deep learning solutions for deforestation monitoring proposed in this work, drawing on the principles of recurrent residual learning discussed in Section 3.3. In this way, in addition to the ability to learn in multiple layers and the mitigation of the problem of vanishing gradients provided by the residual blocks, there will be benefits from the temporal dependency modeling provided by the recurrent layers. The first proposal, illustrated in Figure 5, consists of an adaptation of R2U-Net, using the RRCUs in the encoder and in the bottleneck and the replacement of these units in the decoder by transposed convolutions (TC), as shown in Figure 6. The result is a network with fewer parameters.

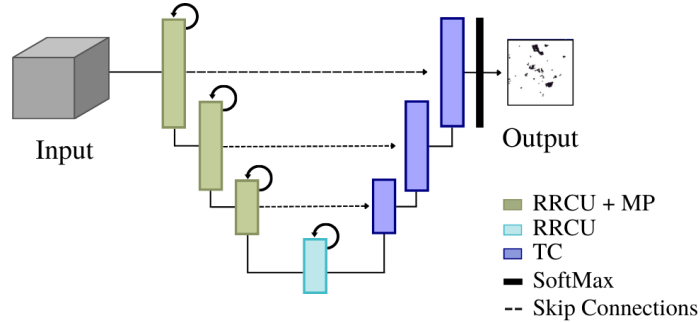


Figure 6: Modified R2U-Net Architecture: RRCNN-1

The second proposal relies on a new recurrent residual block, the Residual Convolutional LSTM block (RCLSTM), that consists of convolutional LSTM blocks with a ReLU activation instead of the RCL used in R2U-Net's RRCU. Figure 7 highlights the differences between the RCLSTM block proposed here and a typical residual block (Figure 7a) and an RRCU block (Figure 7b), already described in Section 3.3.

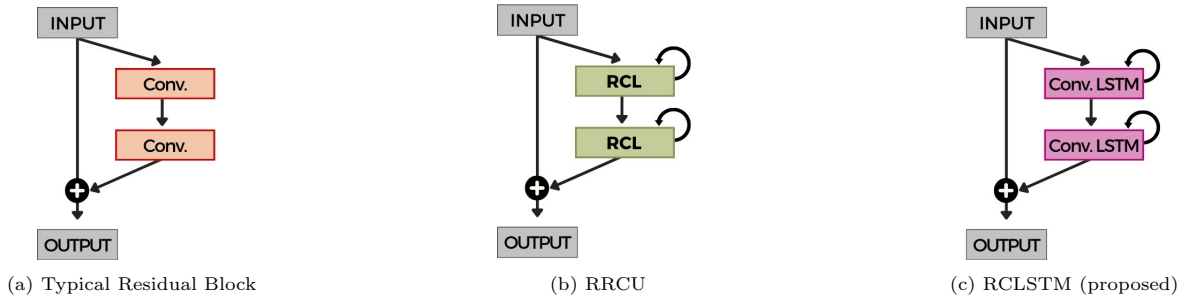


Figure 7: Different variants of residual and recurrent residual convolutional units.

The second proposal derives from the RRCNN-1, replacing the RRCUs by the RCLSTM block in the encoder and bottleneck. Figure 8 depicts the proposed recurrent residual network hereafter called RRCNN-2.

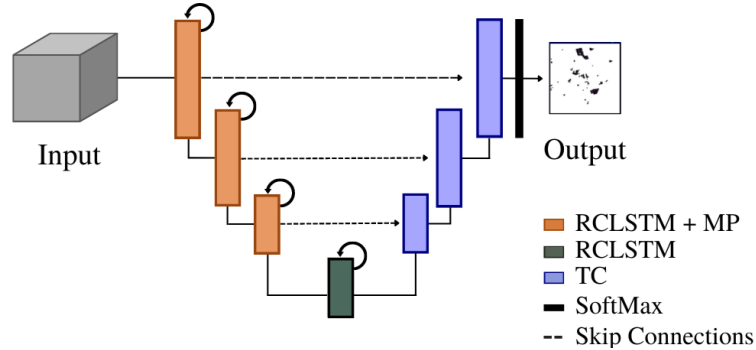


Figure 8: RRCNN-2 Architecture.

The third proposed architecture proposed in this work, named RRCNN-3, is a kind of variant of the prior architecture resulting from replacing the RCLSTM block in the bottleneck with a singular convolutional LSTM block, as depicted in Figure 9.

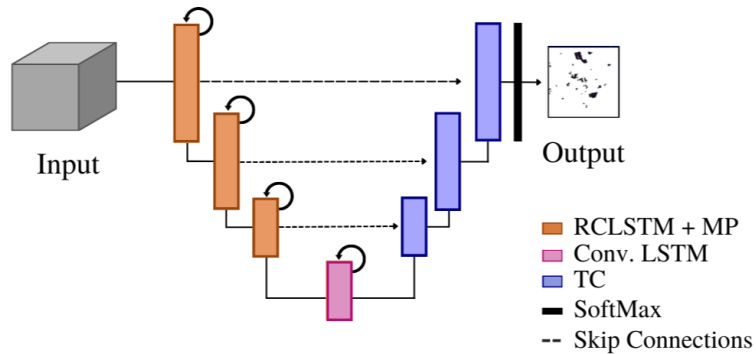


Figure 9: RRCNN-3 Architecture.

5. Experimental Analysis

This section presents the datasets and the experimental setup employed in this study. The deep learning methods presented in Section 3 were used for comparison purposes with the architectures proposed in Section 4.

5.1. Dataset

This study employed Sentinel-1 data from a site in the Brazilian Legal Amazon in the Pará state that extends over $115 \times 186 \text{ Km}^2$. The site is characterized by mixed land cover, mainly dense evergreen forests and pastures (see Figure 10).

To build the input data for the deep learning models described in Section 3 and Section 4, seven images from this same geographical site with resolution of $9327 \times 5767 \times 2$ (width \times height \times polarizations - VV and VH) were captured with a periodicity of approximately two months, starting in August 2019 (Figure 11(a)) and ending in August 2020 (Figure 11(b)).



Figure 10: Geographical location of the study site in the Pará state, Brazil.

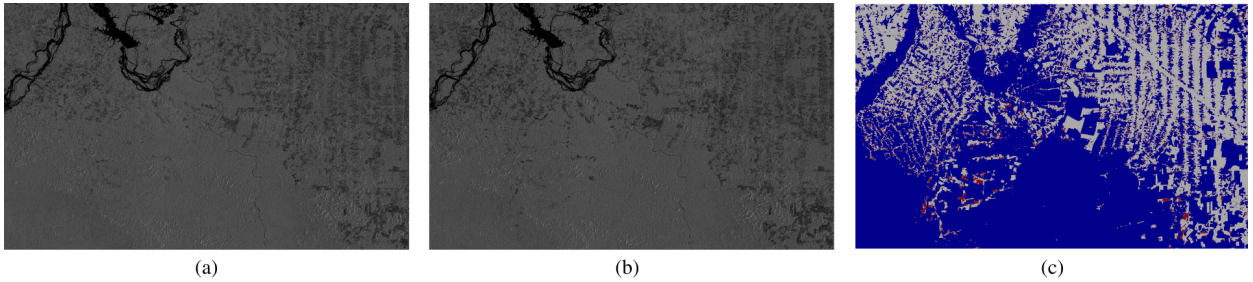


Figure 11: The SAR images: (a) Initial date; (b) Final date; (c) Ground truth of the deforestation that occurred in the period. Legend - gray: past deforestation (1988-2018); red: deforestation (2019-2020); blue: no-deforestation.

The reference map of the deforestation that occurred in this period is available on the INPE website² (Figure 11(c)). It is worth mentioning that this dataset is highly unbalanced, with only 1.06% of the pixels belonging to the deforestation class, 34.04% corresponding to past-deforestation class, and 64.9 % to the no-deforestation class.

The input consists of a tensor $\mathbf{I} \in \mathbf{R}^{H \times W \times 2D}$ resulting from stacking D multitemporal SAR images with 2 polarizations along the third dimension. In our experiments, we explored two scenarios: $D = 2$ to represent the conventional bitemporal set and $D = 7$ to represent an extended multitemporal sequence. Figure 12 shows this process for the bitemporal case.

Each input tensor was splitted into 60 tiles of 932×961 pixels. A cross-validation strategy with six folds was adopted during the training. Each tile was part of the test set only once. Then, the final prediction was a mosaic of all test tiles covering the whole image.

During training and validation the network receives as input tensor patches of 128×128 pixels cropped from the training tiles, with maximum overlap of 70% allowed.

²<http://terrabrasilis.dpi.inpe.br/>

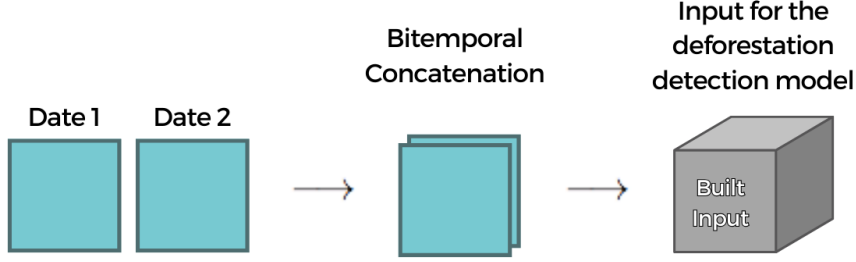


Figure 12: Model Input construction employed for the current experiments. Bitemporal example for data acquired from the same sensor.

5.2. Networks configuration and hyperparameters

The experimental analysis reported in the next section compares the results obtained with the approaches discussed in Section 3, which serve as baselines, with the models proposed in Section 4. Table 1 shows the architectures evaluated in our experiments.

Table 1: Networks Architectures

Architectures	Encoder	Bottleneck	Decoder	Output
U-Net	MP(C(3×3,32))	C(3×3,128)	US(C(3×3,128))	Softmax (C(1×1, #Classes))
	MP(C(3×3,64))	C(3×3,128)	US(C(3×3,64))	
	MP(C(3×3,128))	C(3×3,128)	US(C(3×3,32))	
ResU-Net	MP(RB(3×3,32))	RB(3×3,128)	US(C(3×3,128))	Softmax (C(1×1, #Classes))
	MP(RB(3×3,64))	RB(3×3,128)	US(C(3×3,64))	
	MP(RB(3×3,128))	RB(3×3,128)	US(C(3×3,32))	
R2U-Net	MP(RRCU(3×3,32))	RRCU(3×3,128)	US(RRCU(3×3,128))	Softmax (C(1×1, #Classes))
	MP(RRCU(3×3,64))		US(RRCU(3×3,64))	
	MP(RRCU(3×3,128))		US(RRCU(3×3,32))	
RRCNN-1	MP(RRCU(3×3,32))	RRCU(3×3,128)	TC(3×3,128)	Softmax (C(1×1, #Classes))
	MP(RRCU(3×3,64))		TC(3×3,64)	
	MP(RRCU(3×3,128))		TC(3×3,32)	
RRCNN-2	MP(RCLSTM(3×3,32))	RCLSTM(3×3,128)	TC(3×3,128)	Softmax (C(1×1, #Classes))
	MP(RCLSTM(3×3,64))		TC(3×3,64)	
	MP(RCLSTM(3×3,128))		TC(3×3,32)	
RRCNN-3	MP(RCLSTM(3×3,32))	Conv. LSTM(3×3,128)	TC(3×3,128)	Softmax (C(1×1, #Classes))
	MP(RCLSTM(3×3,64))		TC(3×3,64)	
	MP(RCLSTM(3×3,128))		TC(3×3,32)	

The parametrization is (Kernel Height x Kernel Width, Number of filters). Symbols: C (Convolution), MP (Max-pooling), RB (Residual Block), US (Up-sampling), TC (Transpose Convolution), RRCU (Recurrent Residual Convolutional Unit), RCLSTM (Residual Convolutional LSTM block).

The employed parameter setup follows: batch size equal to 32, Adam optimizer with learning rate equal to $1e^{-3}$, and β equal to 0.9, and, to avoid over-fitting, an early stopping strategy with patience equal to 10.

Considering that the dataset is highly unbalanced, the employed loss function was the weighted categorical cross entropy, given by Ho & Wookey (2019):

$$\text{Loss}_{wce} = -\frac{1}{M} \sum_{k=1}^K \sum_{m=1}^M w_k \cdot y_m^k \cdot \log(\hat{y}_m^k), \quad (11)$$

where M is the number of training pixels, K is the number of classes, w_k is the weight for class k , y_m^k is the target label for training example m for class k , x_m is the input for training example m and \hat{y}_m^k refers to the predicted probability for training example m for class k .

In the present case, adopted the weights 0.2 for class no-deforestation and 0.8 for class deforestation. Following the PRODES methodology, the past deforestation class was ignored during training, validation, and testing. Only patches having at least 2% of pixels of the deforestation class were used for training. In addition, a data augmentation procedure was applied for training and validation; these operations included rotation (multiples of 90°) and flipping (horizontal, vertical) transformations. The threshold to separate the deforestation and no-deforestation classes was 50%.

5.3. Evaluation metrics

The generated deforestation maps classify each pixel into categories of deforestation and no-deforestation. Designating deforestation as a “positive” and no-deforestation as “negative”, there are four possible outcomes: true positive (TP) being a correctly identified deforestation/positive, true negative (TN) being a correctly identified no-deforestation, false positive (FP) being an unchanged pixel labeled as deforestation and false negative (FN) a changed pixel labeled as no-deforestation.

Among the several performance metrics that have been used to evaluate the results of a deforestation detection process, three of the most common are Precision, Recall, and F1-Score, as can be seen in the studies mentioned in Section 2 and also in review articles about change detection with remote sensing data (Parelius, 2023; Shafique et al., 2022).

The Precision metric denotes the ratio between the number of correctly classified deforestation pixels and the total number of pixels identified as deforestation.

$$\text{Precision} = \frac{TP}{TP + FP}. \quad (12)$$

The Recall metric, conversely, is equivalent to the true positive rate, representing the ratio of accurately classified deforestation pixels to the total number of original deforestation pixels.

$$\text{Recall} = \frac{TP}{TP + FN}. \quad (13)$$

With Recall and Precision, the F1-Score is calculated as follows:

$$\text{F1-Score} = \frac{2 \cdot \text{Precision} \cdot \text{Recall}}{\text{Precision} + \text{Recall}}. \quad (14)$$

5.4. Computational Resources

The preliminary experiments were conducted on the following system configuration:

- Processor: Thirty-Two-Core AMD Ryzen™ Threadripper™ PRO 5975WX Processor - 3.60GHz 128MB L3 Cache (280W)
- Memory: 8 x 64GB PC4-25600 3200MHz DDR4 ECC RDIMM (512GB total)
- GPU Accelerators: 3 x NVIDIA® RTX A6000 - 48GB GDDR6 - PCIe 4.0 x16
- Operating System: Ubuntu 22.04.2 LTS

The use of all GPUs available on the machine for training was enabled by the Mirrored Strategy (`tf.distribute.MirroredStrategy`³) function of the TensorFlow deep learning framework. This data parallelism approach is intended to accelerate the training process by allowing a deep learning model to be replicated across multiple GPUs, where each GPU retains a full copy of the model. During training, each replica processes a portion of the training data, and then gradient updates are synchronized between GPUs to update the global model. According to Pang et al. (2020), using this function further accelerates training and allows for larger models by leveraging memory from multiple GPUs.

³Available on https://www.tensorflow.org/api_docs/python/tf/distribute/MirroredStrategy

6. Experimental Results

In this section, we delve into the findings derived from our experimental analysis to evaluate the performance of the deforestation detection architectures outlined in Section 4. Figures 13 through 15 showcase the performance metrics of the methods introduced in this study, alongside those referenced in Section 3, which serve as our baseline for comparison. These figures provide a comprehensive assessment of accuracy, encompassing Precision, Recall, and F1-score, derived from experiments on both bitemporal and multitemporal input data. The reported scores have been derived using K-fold cross-validation with a value of $K = 6$, following the methodology detailed in Section 5.2.

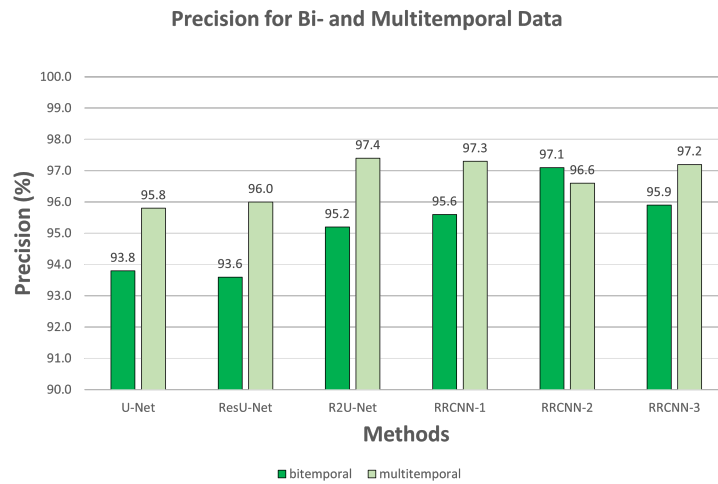


Figure 13: Comparison of methods in terms of Precision for bitemporal and multitemporal data

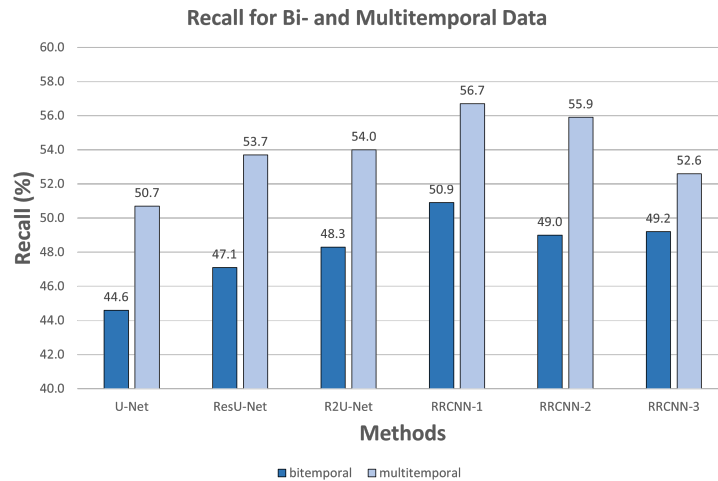


Figure 14: Comparison of methods in terms of Recall for bitemporal and multitemporal data

The first finding that emerges from the analysis of the figures is that all performance metrics derived from multi-temporal data consistently outperformed those obtained from bi-temporal data. Notably, the only exception was the Precision for RRCNN-2, which declined by a small amount for the multitemporal data. This observation corroborates the hypothesis that signs of change in SAR images get less apparent

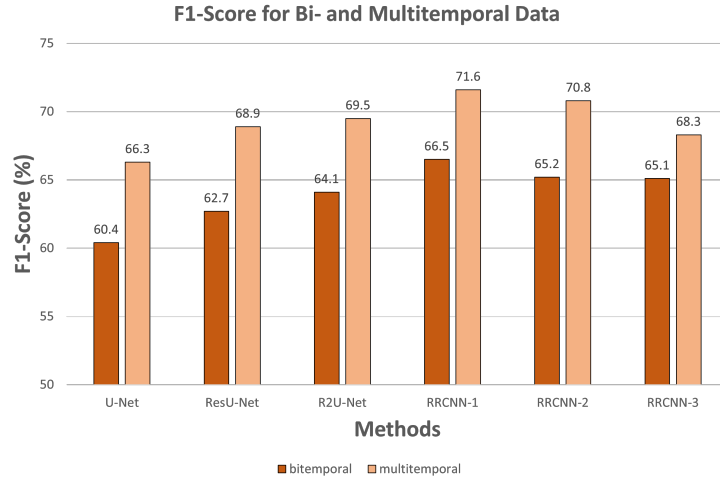


Figure 15: Comparison of methods in terms of F1-Score for bitemporal and multitemporal data

with time. Consequently, using a sequence rather than a mere pair of SAR images improves the chance of capturing changes that occur during the target observation interval.

The second conclusion from our experiments is that recurrent variants, namely the R2U-Net and the three RRCNN variants, consistently outperformed their strictly convolutional counterparts, namely U-Net and ResU-Net. This trend was apparent in all three metrics we examined.

As for the three proposed variants, the RRCNN-1 consistently outperformed the other two, with RRCNN-2 holding a slight edge over RRCNN-3. Remarkably, RRCNN-1 showcased the best results among all the architectures we examined, surpassing the top-performing baseline, the R2U-Net, by 2% in F1-Score.

Another aspect deserving of examination is the computational efficiency. Figure 16 provides insight into the count of trainable parameters associated with each scrutinized configuration.

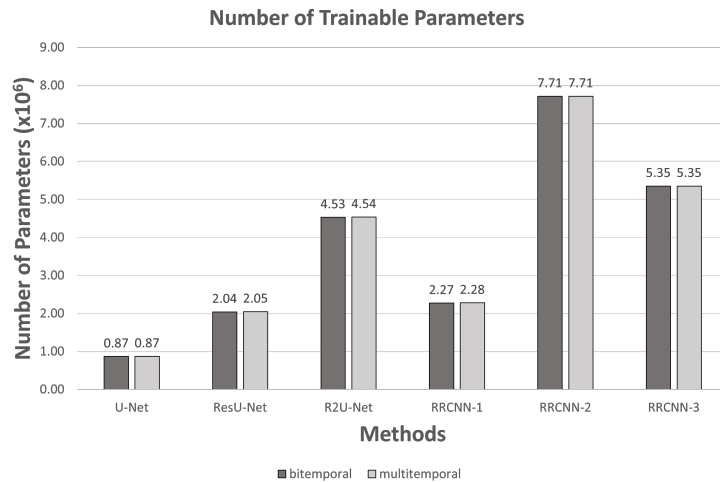


Figure 16: Number of Parameters of each model for the bitemporal and multitemporal data

By looking at each bar group in Figure 16, one observes that adopting a sequence of images instead of a mere image pair had a marginal impact on the parameter count for each model. It is also observed that the RRCNN-2 and RRCNN-3 were the variants with the largest parameter count, followed closely by R2U-Net.

Interestingly RRCNN-1 stands out by carrying approximately half the number of parameters when

contrasted with R2U-Net, bringing it close to the parameter count of ResU-Net. This implies that RRCNN-1 successfully incorporates recurrence into its model framework with minimal alterations to the overall parameter load compared to ResU-Net, a fully convolutional network.

Figure 17 and Figure 18 show the training and inference times. By and large, as expected, these Figures show a profile similar to those of the parameter values.

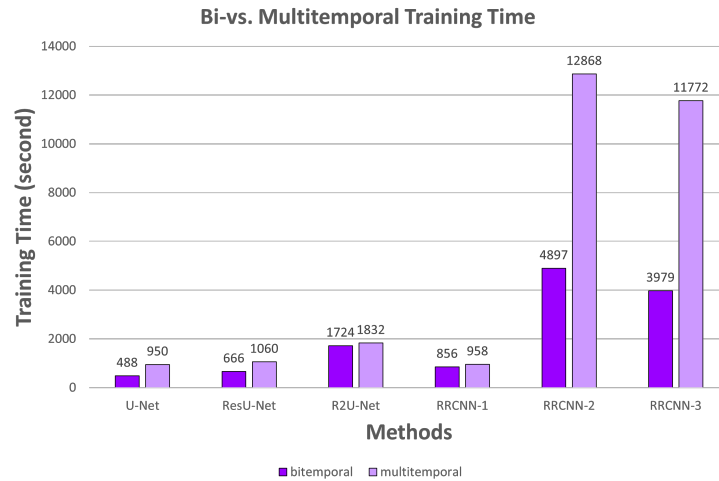


Figure 17: Training Time of each model for bitemporal and multitemporal data

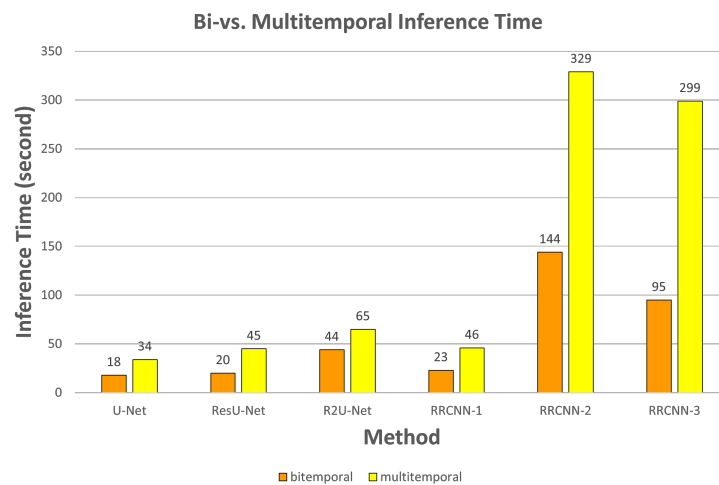


Figure 18: Inference Time of each model for bitemporal and multitemporal data

As observed in Figures 13 through 15 together with Figures 17 - 18, RRCNN-1 very clearly presented the best compromise between accuracy and computational efficiency. Among the variants analyzed, RRCNN-1 presented the best accuracy, and, on the other hand, processing times, particularly the inference time, were close to that of the fastest network, the U-Net.

To evaluate the deforestation maps generated in the experiments, Figure 19 illustrates the change maps produced in each experiment in snips of the target site. Each row refers to a different architecture, and each column shows the results for a different snip obtained with the bitemporal and multitemporal inputs.

As observed in Figure 19 the false positive spots are minimal, being noticed only in minor regions, mainly in maps generated with bitemporal input (Figure 19-(g), (k), (o), (s) and (w)) and even smaller spots in

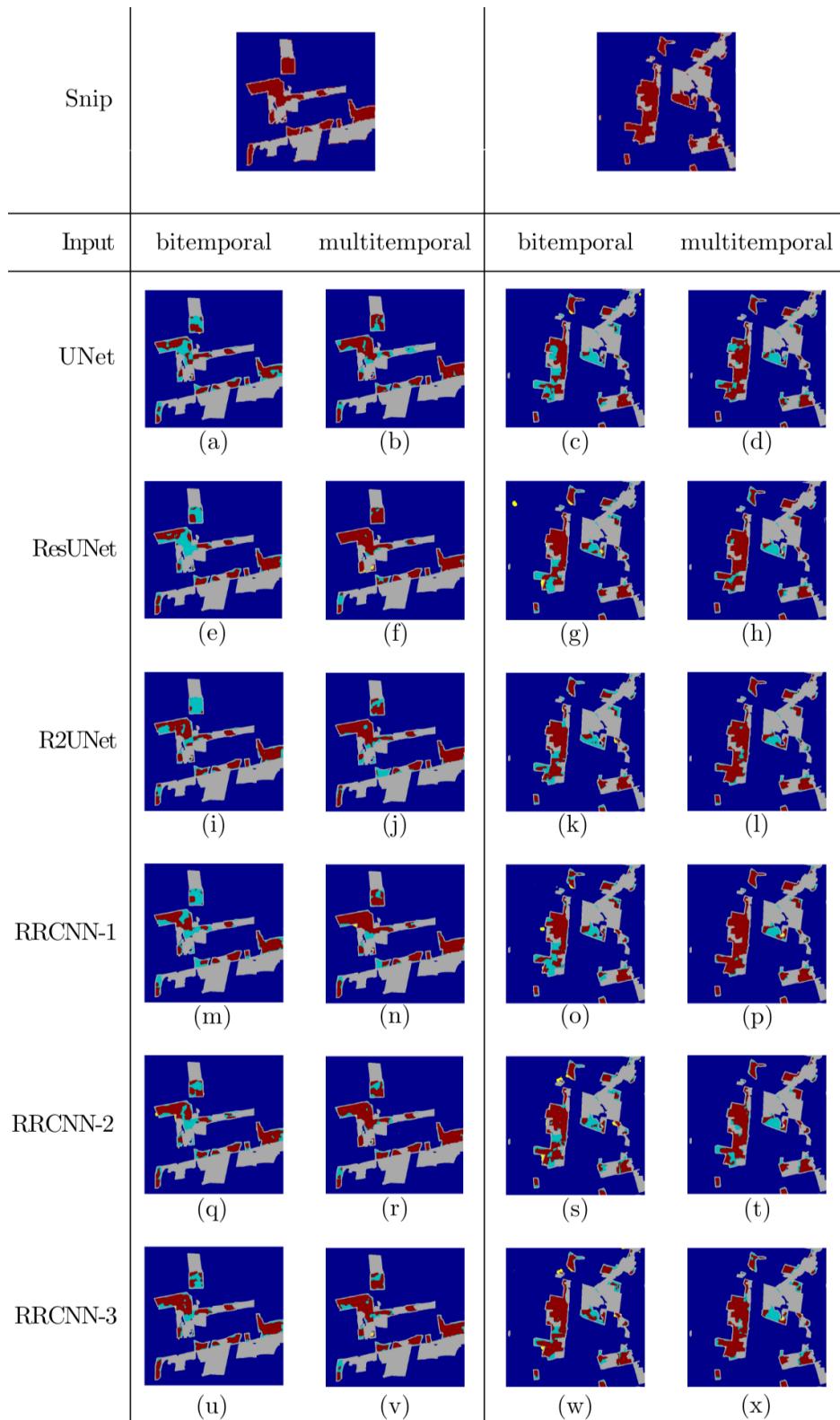


Figure 19: Predicted deforestation maps in two snips from the test set. Legend - past deforestation; deforestation (true positives); no deforestation (true negatives); false positives; false negatives.

Figure 19-(p) and (v), that represent maps generated with a multitemporal input.

Regarding false negative spots, their decrease is noticed in the maps generated with multitemporal inputs in relation to bitemporal inputs, confirming the quantitative results. The change map generated by the RRCNN-1 with the multitemporal input was the closest to the ground-truth, as can be seen in Figure 19(p). The other developed architectures, RRCNN-2 and RRCNN-3, also delivered well defined maps.

7. Conclusions and Future Work

The present research seeks for developing solutions for deforestation monitoring using deep learning approaches. Until the present stage of this investigation, three change detection architectures relying on recurrent residual learning have been formulated, RRCNN-1, RRCNN-2 and RRCNN-3. These methods were compared with three techniques from the literature, U-Net, ResU-Net and R2U-Net, the latter being a residual recurrent network.

Preliminary experiments were conducted using Sentinel-1 SAR images corresponding to a region of the Brazilian Amazon rainforest. The ground-truth used in this work was collected from the PRODES Project, which was developed by the National Institute for Space Research (INPE). The performance of the techniques was compared using bitemporal data, which are usually emphasized in the literature reports, and also multitemporal data.

RRCNN-1 presented the best performance in most metrics, achieving a F1-Score of 66,5% with the bitemporal input and 71,6% with the multitemporal input. RRCNN-2 had the best Precision (97,1%), the second best F1-Score (65,2%) and the third best Recall (49,0%) with the bitemporal input and the second best Recall and F1-Score with the multitemporal input, 55,9% and 70,8%, respectively. RRCNN-3 achieved the second best Recall (49,2%) and Precision (95,9%) in the bitemporal case and the third best Precision (97,2%) with the multitemporal input.

Based on the assessed metrics and the change maps generated through the tested networks, it became evident that the incorporation of an extended sequence of images significantly enhanced the deforestation detection performance, highlighting the potential benefits of incorporating a comprehensive longer temporal context in the analysis. RRCNN-1, particularly, delivered significant improved results with a multitemporal input compared to the bitemporal case, while incurring a training time increase of nearly 2 minutes.

The RRCNN-2 and RRCNN-3 networks are designed with ConvLSTM layers in their architectures, which led to longer training and inference times. This is attributed to the inherently high computational complexity associated with LSTM operations, resulting in more demanding computational resources during the learning process.

The next steps for this research include tests with other datasets commonly employed in deforestation detection surveys.

Acknowledgments

The authors would like to thank the financial support provided by CNPq, CAPES and FAPERJ.

References

- Alom, M. Z., Yakopcic, C., Hasan, M., Taha, T. M., & Asari, V. K. (2019). Recurrent residual u-net for medical image segmentation. *Journal of Medical Imaging*, 6, 014006–014006.
- Amin, A., Choumert-Nkolo, J., Combes, J.-L., Motel, P. C., Kéré, E. N., Ongono-Olinga, J.-G., & Schwartz, S. (2019). Neighborhood effects in the brazilian amazônia: Protected areas and deforestation. *Journal of Environmental Economics and Management*, 93, 272–288.
- Asokan, A., & Anitha, J. (2019). Change detection techniques for remote sensing applications: A survey. *Earth Science Informatics*, 12, 143–160.

- Bai, T., Wang, L., Yin, D., Sun, K., Chen, Y., Li, W., & Li, D. (2022). Deep learning for change detection in remote sensing: a review. *Geo-spatial Information Science*, (pp. 1–27).
- Ban, Y., & Yousif, O. (2016). Change detection techniques: A review. *Multitemporal remote sensing: methods and applications*, (pp. 19–43).
- Basavaraju, K., Sravya, N., Lal, S., Nalini, J., Reddy, C. S., & Dell’Acqua, F. (2022). Ucdnet: A deep learning model for urban change detection from bi-temporal multispectral sentinel-2 satellite images. *IEEE Transactions on Geoscience and Remote Sensing*, *60*, 1–10.
- Calin, O. (2020). *Deep Learning Architectures*. Cham, Switzerland: Springer Nature.
- Chen, H., Qi, Z., & Shi, Z. (2021). Remote sensing image change detection with transformers. *IEEE Transactions on Geoscience and Remote Sensing*, *60*, 1–14.
- Dawelbait, M., & Morari, F. (2012). Monitoring desertification in a savannah region in sudan using landsat images and spectral mixture analysis. *Journal of Arid Environments*, *80*, 45–55.
- De Bem, P. P., de Carvalho Junior, O. A., Fontes Guimarães, R., & Trancoso Gomes, R. A. (2020). Change detection of deforestation in the brazilian amazon using landsat data and convolutional neural networks. *Remote Sensing*, *12*, 901.
- Diniz, J. M. F. d. S., Gama, F. F., & Adami, M. (2022). Evaluation of polarimetry and interferometry of sentinel-1a sar data for land use and land cover of the brazilian amazon region. *Geocarto International*, *37*, 1482–1500.
- Doblas, J., Shimabukuro, Y., Sant’Anna, S., Carneiro, A., Aragão, L., & Almeida, C. (2020). Optimizing near real-time detection of deforestation on tropical rainforests using sentinel-1 data. *Remote Sensing*, *12*, 3922.
- Fang, Y., Zhai, Q., Zhang, Z., & Yang, J. (2023). Change point detection for fine-grained mfr work modes with multi-head attention-based bi-lstm network. *Sensors*, *23*, 3326.
- Giljum, S., Maus, V., Kuschig, N., Luckeneder, S., Tost, M., Sonter, L. J., & Bebbington, A. J. (2022). A pantropical assessment of deforestation caused by industrial mining. *Proceedings of the National Academy of Sciences*, *119*, e2118273119.
- Goodfellow, I., Bengio, Y., & Courville, A. (2016). *Deep learning*. MIT press.
- Graves, A. (2013). Generating sequences with recurrent neural networks. *arXiv preprint arXiv:1308.0850*, .
- Han, X., Zhong, Y., Cao, L., & Zhang, L. (2017). Pre-trained alexnet architecture with pyramid pooling and supervision for high spatial resolution remote sensing image scene classification. *Remote Sensing*, *9*, 848.
- He, K., Zhang, X., Ren, S., & Sun, J. (2016). Deep residual learning for image recognition. In *Proceedings of the IEEE conference on computer vision and pattern recognition* (pp. 770–778).
- Hethcoat, M. G., Carreiras, J., Edwards, D., Bryant, R. G., & Quegan, S. (2020). Detecting tropical selective logging with sar data requires a time series approach. *bioRxiv*, (pp. 2020–03).
- Ho, Y., & Wookey, S. (2019). The real-world-weight cross-entropy loss function: Modeling the costs of mislabeling. *IEEE access*, *8*, 4806–4813.
- Hochreiter, S., & Schmidhuber, J. (1997). Long short-term memory. *Neural computation*, *9*, 1735–1780.
- Khankeshizadeh, E., Mohammadzadeh, A., Moghimi, A., & Mohsenifar, A. (2022). Fcd-r2u-net: Forest change detection in bi-temporal satellite images using the recurrent residual-based u-net. *Earth Science Informatics*, *15*, 2335–2347.

- Khelifi, L., & Mignotte, M. (2020). Deep learning for change detection in remote sensing images: Comprehensive review and meta-analysis. *Ieee Access*, *8*, 126385–126400.
- Kou, C., Li, W., Liang, W., Yu, Z., & Hao, J. (2019). Microaneurysms segmentation with a u-net based on recurrent residual convolutional neural network. *Journal of Medical Imaging*, *6*, 025008–025008.
- Li, Z., Yan, C., Sun, Y., & Xin, Q. (2022). A densely attentive refinement network for change detection based on very-high-resolution bitemporal remote sensing images. *IEEE Transactions on Geoscience and Remote Sensing*, *60*, 1–18.
- Liang, M., & Hu, X. (2015). Recurrent convolutional neural network for object recognition. In *Proceedings of the IEEE conference on computer vision and pattern recognition* (pp. 3367–3375).
- Ling, J., Hu, L., Cheng, L., Chen, M., & Yang, X. (2022). Ira-mrsnet: A network model for change detection in high-resolution remote sensing images. *Remote Sensing*, *14*, 5598.
- Masolele, R. N., De Sy, V., Herold, M., Marcos, D., Verbesselt, J., Gieseke, F., Mullissa, A. G., & Martius, C. (2021). Spatial and temporal deep learning methods for deriving land-use following deforestation: A pan-tropical case study using landsat time series. *Remote Sensing of Environment*, *264*, 112600.
- Moustafa, M. S., Mohamed, S. A., Ahmed, S., & Nasr, A. H. (2021). Hyperspectral change detection based on modification of unet neural networks. *Journal of Applied Remote Sensing*, *15*, 028505–028505.
- Mubashar, M., Ali, H., Grönlund, C., & Azmat, S. (2022). R2u++: a multiscale recurrent residual u-net with dense skip connections for medical image segmentation. *Neural Computing and Applications*, *34*, 17723–17739.
- Nair, V., & Hinton, G. E. (2010). Rectified linear units improve restricted boltzmann machines. In *Proceedings of the 27th international conference on machine learning (ICML-10)* (pp. 807–814).
- Newbold, T., Hudson, L. N., Hill, S. L., Contu, S., Lysenko, I., Senior, R. A., Börger, L., Bennett, D. J., Choimes, A., Collen, B. et al. (2015). Global effects of land use on local terrestrial biodiversity. *Nature*, *520*, 45–50.
- Nicolau, A. P., Flores-Anderson, A., Griffin, R., Herndon, K., & Meyer, F. J. (2021). Assessing sar c-band data to effectively distinguish modified land uses in a heavily disturbed amazon forest. *International Journal of Applied Earth Observation and Geoinformation*, *94*, 102214.
- Ortega, M. X., Feitosa, R. Q., Bermudez, J. D., Happ, P. N., & De Almeida, C. A. (2021). Comparison of optical and sar data for deforestation mapping in the amazon rainforest with fully convolutional networks. In *2021 IEEE International Geoscience and Remote Sensing Symposium IGARSS* (pp. 3769–3772). IEEE.
- Pang, B., Nijkamp, E., & Wu, Y. N. (2020). Deep learning with tensorflow: A review. *Journal of Educational and Behavioral Statistics*, *45*, 227–248.
- Panuju, D. R., Paull, D. J., & Griffin, A. L. (2020). Change detection techniques based on multispectral images for investigating land cover dynamics. *Remote Sensing*, *12*, 1781.
- Papadomanolaki, M., Verma, S., Vakalopoulou, M., Gupta, S., & Karantza, K. (2019). Detecting urban changes with recurrent neural networks from multitemporal sentinel-2 data. In *IGARSS 2019-2019 IEEE international geoscience and remote sensing symposium* (pp. 214–217). IEEE.
- Parelius, E. J. (2023). A review of deep-learning methods for change detection in multispectral remote sensing images. *Remote Sensing*, *15*, 2092.
- Peng, D., Zhang, Y., & Guan, H. (2019). End-to-end change detection for high resolution satellite images using improved unet++. *Remote Sensing*, *11*, 1382.

- Perbet, P., Fortin, M., Ville, A., & Béland, M. (2019). Near real-time deforestation detection in malaysia and indonesia using change vector analysis with three sensors. *International Journal of Remote Sensing*, *40*, 7439–7458.
- Reis, M. S., Dutra, L. V., Sant’Anna, S. J. S., & Escada, M. I. S. (2020). Multi-source change detection with palsar data in the southern of para state in the brazilian amazon. *International Journal of Applied Earth Observation and Geoinformation*, *84*, 101945.
- Rumelhart, D. E., Hinton, G. E., & Williams, R. J. (1986). Learning representations by back-propagating errors. *nature*, *323*, 533–536.
- Shafique, A., Cao, G., Khan, Z., Asad, M., & Aslam, M. (2022). Deep learning-based change detection in remote sensing images: A review. *Remote Sensing*, *14*, 871.
- Shi, C., Zhang, Z., Zhang, W., Zhang, C., & Xu, Q. (2022). Learning multiscale temporal–spatial–spectral features via a multipath convolutional lstm neural network for change detection with hyperspectral images. *IEEE Transactions on Geoscience and Remote Sensing*, *60*, 1–16.
- Shi, W., Zhang, M., Zhang, R., Chen, S., & Zhan, Z. (2020). Change detection based on artificial intelligence: State-of-the-art and challenges. *Remote Sensing*, *12*, 1688.
- Singh, A. (1989). Review article digital change detection techniques using remotely-sensed data. *International journal of remote sensing*, *10*, 989–1003.
- Stauffer, M., & McKinney, R. (1978). *Landsat image differencing as an automated land cover change detection technique*. Technical Report.
- Sule, S. D., & Wood, A. (2020). Application of principal component analysis to remote sensing data for deforestation monitoring. In *Remote Sensing for Agriculture, Ecosystems, and Hydrology XXII* (pp. 17–29). SPIE volume 11528.
- Valeriano, D. M., Mello, E. M., Moreira, J. C., Shimabukuro, Y. E., Duarte, V., Souza, I., Santos, J., Barbosa, C. C., & Souza, R. (2004). Monitoring tropical forest from space: the prodes digital project. *International Archives of Photogrammetry Remote Sensing and Spatial Information Sciences*, *35*, 272–274.
- Wang, G., Li, B., Zhang, T., & Zhang, S. (2022). A network combining a transformer and a convolutional neural network for remote sensing image change detection. *Remote Sensing*, *14*, 2228.
- Wang, Y., & Tian, F. (2016). Recurrent residual learning for sequence classification. In *Proceedings of the 2016 conference on empirical methods in natural language processing* (pp. 938–943).
- Yue, B., Fu, J., & Liang, J. (2018). Residual recurrent neural networks for learning sequential representations. *Information*, *9*, 56.
- Zhang, Z., Liu, Q., & Wang, Y. (2018). Road extraction by deep residual u-net. *IEEE Geoscience and Remote Sensing Letters*, *15*, 749–753.
- Zhao, W., Chen, X., Ge, X., & Chen, J. (2020). Using adversarial network for multiple change detection in bitemporal remote sensing imagery. *IEEE Geoscience and Remote Sensing Letters*, *19*, 1–5.
- Zheng, Z., Wan, Y., Zhang, Y., Xiang, S., Peng, D., & Zhang, B. (2021a). Clnet: Cross-layer convolutional neural network for change detection in optical remote sensing imagery. *ISPRS Journal of Photogrammetry and Remote Sensing*, *175*, 247–267.
- Zheng, Z., Zhong, Y., Wang, J., Ma, A., & Zhang, L. (2021b). Building damage assessment for rapid disaster response with a deep object-based semantic change detection framework: From natural disasters to man-made disasters. *Remote Sensing of Environment*, *265*, 112636.